Macromolecular Chemistry and Physics
www.mcp-journal.de

Exerting Additive-Assisted Morphological Control during Hydrothermal Polymerization

*M. Josef Taublaender, Manuel Reiter, and Miriam M. Unterlass**

Hydrothermal polymerization (HTP) is a benign and inherently green synthetic approach to synthesize highly crystalline polyimides (PIs) in nothing but high-temperature water (HTW). In a typical HTP experiment, highly crystalline PI microparticles of sheet-like as well as flower-like morphology are obtained. Within this contribution, the effect of four additives (PEG400, PEG8000, P123, CTAB) on the crystallinity and morphology of the PI poly(*p*-phenylene pyromellitimide) is investigated. From the experiments performed, it becomes evident that the type as well as the concentration of additive heavily influences morphology. However, even the highest tested concentration of additive (67 g L^{-1} of PEG8000) does not lead to a change in average crystallinity, as determined from powder X-ray diffraction. Hence, this approach provides a straightforward method to intentionally tune PI particle morphology without losing the outstanding materials properties generated by the high crystallinity obtained via HTP. Additionally, a hypothesis regarding the poly(ethylene glycol)-induced morphology alteration is presented.

1. Introduction

The synthesis of compounds by environmentally friendly, nontoxic and efficient routes—summarized by the term "green chemistry"—has gained great importance in recent years.[1] The relevance and timeliness of green chemistry stands on the growing awareness for health and the environment. This is underlined by an increasing number of governmental regulations such as the REACH—the *Regulation (EC) No 1907/2006 of the European Parliament and of the Council of 18 December 2006 concerning the Registration, Evaluation, Authorization and Restriction of Chemicals*.[2] Such regulations are more pressing for industrial production plants than for (academic) research laboratories. Therefore, it is fair to say that for chemical compounds, which are already produced at an industrial scale, green syntheses and processing are heavily sought after. Polymers are one of the biggest fractions of chemical production. For instance, in 2016 polymers accounted for 20% of the overall chemical sales in the EU.[3] Clearly, the development of green syntheses toward such an important class of compounds is a topic of the utmost importance. To date only a limited number of green polymerization techniques is known:[4] (i) Enzymatic polymerizations, which employ isolated enzymes as in vitro polymerization catalysts. Hence, they replace conventional catalysts, which are often toxic or made up of scarce elements.[4,5] (ii) Photopolymerization is considered a green route, since the monomer formulations used are typically solvent-free resins. Furthermore, low energy input as well as low reaction temperatures are required.[6] (iii) Hydrothermal polymerization (HTP) employs solely H_2O as a solvent at elevated temperatures and pressures without the need for catalysts or promotors.[4] Aside its green nature HTP generates outstandingly crystalline products. This feature is highly promising, since for being realistically implemented green syntheses must generate at least equal or even superior materials properties compared to those obtained by classical routes. For a given material crystallinity is increasing both the chemical and the thermal stability, because in order to chemically or thermally degrade the material the lattice energy has to be furnished in addition to the sum of bonding energies.[7]

The generation of highly crystalline compounds under hydrothermal conditions is a typical mineral formation process. For instance, natural zeolites are exclusively generated hydrothermally. Therefore, HTP is termed a geomimetic polycondensation.[8,9] To date HTP has been exclusively reported for the preparation of polyimides (PIs),[8,10,11] and PI/SiO_2 hybrid materials.[12] In a typical HTP experiment, the comonomers toward PIs, i.e., a diamine and a dianhydride (typically employed as the corresponding tetracarboxylic acid) are mixed in H_2O at RT ≤ T < 100 °C (**Figure 1**A). Due to the protic polar environment, the comonomers rapidly react to a monomer salt via acid–base reaction between the CO_2H and the NH_2 functions (Figure 1A).[8,13] Monomer salts of the diammonium–dicarboxylate dicarboxylic acid type are typically insoluble in H_2O at RT. Therefore, at RT the monomer salt and H_2O form a dispersion. For generating hydrothermal conditions (H_2O at T > 100 °C and p > 1 bar) the monomer salt dispersion is placed in a pressure vessel, aka autoclave (Figure 1B), and heated to the reaction temperature T_R > 100 °C. Since the autoclave is a closed system, increased p builds up autogenously. The system is best described as the concurrence of $H_2O_{(l)}$ continuously evaporating and $H_2O_{(g)}$ continuously condensing. For pure H_2O this corresponds to the liquid–vapor coexistence area in the (p,T,V)

M. J. Taublaender, M. Reiter, Dr. M. M. Unterlass
TU Wien, Institute of Materials Chemistry
Getreidemarkt 9, 1060 Vienna, Austria
E-mail: miriam.unterlass@tuwien.ac.at

The ORCID identification number(s) for the author(s) of this article can be found under https://doi.org/10.1002/macp.201700397.

DOI: 10.1002/macp.201700397

phase diagram (Figure 1C).[14] The physicochemical properties of high-temperature water (HTW) are strongly different from H_2O at RT.[7] Most important for HTP are: (i) the decrease in viscosity (η) and density (ρ) with T, which is highly beneficial for diffusion-controlled reactions; (ii) the decrease in the static dielectric constant (ε) with T, which allows for dissolving organic (mostly aromatic) monomers; and (iii) the ionic product K_w (the product of the concentrations of hydronium ions and hydroxide ions), which reflects the ability of H_2O to act as acid/base, increases with T until a maximum at 250 °C, where K_w is three orders of magnitude higher than at RT.[7] This high K_W translates into H_2O itself acting as acid, base, and even potent acido-basic bicatalyst. Since cyclization condensation reactions of amines with 1,2-dicarboxylic acids toward cyclic imides require promotion through an acid or a base, HTW is an ideal medium for the formation of polyimides. Both the decrease in η, ρ, and ε and the increase in K_w are a consequence of H_2O's hydrogen bonding network breaking down with T (Figure 1D): While at 25 °C one finds an average of 3.9 H-bonds per molecule of H_2O, only an average of 2.4 H-bonds is present at 300 °C. Note that these properties scale strongly with T, and only very little with p in $H_2O_{(l)}$, and that the changes in these properties are minute for H_2O vapor.

HTP generates highly crystalline PIs: the powder X-ray diffraction (PXRD) patterns typically show little to no amorphous halos at all, and PI crystal structures could be refined from PXRD data for to date three hydrothermally polymerized PIs.[8,10,11] The outstanding crystallinity is nicely reflected in their morphology, which for fully aromatic PIs is best described as flower- and platelet-shaped microparticles.[8,10,11]

With this contribution, we have set out to exert morphological control over PIs from HTP. The motivation here is that particles of different shapes will have different surface areas. First, this has tremendous implications for potential application as particulate additives, e.g., in paints (higher particle surface area generates more contact with the medium at good wetting). Second, the particle surface areas are extremely important for industrial production, especially for process steps such as powder drying. Since HTP is using H_2O as reaction medium, a plethora of (at room temperature) water-soluble additives can be employed as morphology-modifying agents. For this study, we have investigated the use of four different additives, namely of poly(ethylene glycol) (PEG) of two different average molecular weights, the poly(ethylene glycol)–poly(propylene glycol)–poly(ethylene glycol) triblock copolymer Pluronic P123, and the low-molecular-weight surfactant cetyl trimethyl ammonium bromide (CTAB). We herein study the impact of these additives on morphology and crystallinity of poly(*p*-phenylene pyromellitimide), PPPI, synthesized via HTP.

2. Experimental Section

2.1. Chemicals

p-Phenylenediamine (PDA, 97%; Sigma-Aldrich) and pyromellitic dianhydride (PMDA, 98%; Sigma-Aldrich), CTAB (98%; Sigma-Aldrich), PEG with an average molecular weight ($\overline{M_n}$) of 400 g mol^{-1} (PEG400; Sigma-Aldrich), PEG with an $\overline{M_n}$ of 8000 g mol^{-1} (PEG8000; Applichem), poly(ethylene glycol)-*block*-poly(propylene glycol)-*block*-poly(ethylene glycol) Pluronic P123 (P123; Sigma-Aldrich) were purchased commercially and used as received.

M. Josef Taublaender studied technical chemistry at TU Wien (AT). He completed his B.Sc. thesis in the field of macromolecular chemistry. During his master's studies, M.J.T. spent an exchange semester at the University of Florida in Gainesville (US). After returning to TU Wien, he completed his M.Sc. thesis in the group of Miriam M. Unterlass, dealing with novel synthetic methods for high-performance polymers. Since March 2017, M.J.T. is pursuing his Ph.D. work under the supervision of Miriam M. Unterlass, focusing on green syntheses of high-performance materials.

Manuel Reiter is studying technical chemistry at TU Wien (AT) since 2014. He is currently working on his B.Sc. thesis under the supervision of Miriam M. Unterlass. His thesis deals with the intentional morphological tuning of polyimide microparticles.

Miriam M. Unterlass studied chemistry, process engineering, and materials science in Würzburg (DE), Southampton (UK), and Lyon (FR), and obtained her Ph.D. at the Max Planck Institute of Colloids and Interfaces in Golm (DE) in the group of Markus Antonietti. M.M.U. then worked for one year as a postdoc with Ludwik Leibler at the ESPCI in Paris (FR). In 2012, she became group leader at the Institute of Materials Chemistry at TU Wien (AT). In 2017, M.M.U. was awarded a START prize by the Austrian Science Fund (FWF). Her group is working on nonclassical synthetic approaches toward advanced materials, with a focus on green polymerization techniques, efficient materials synthesis via precursor preorganization and crystalline organic materials.

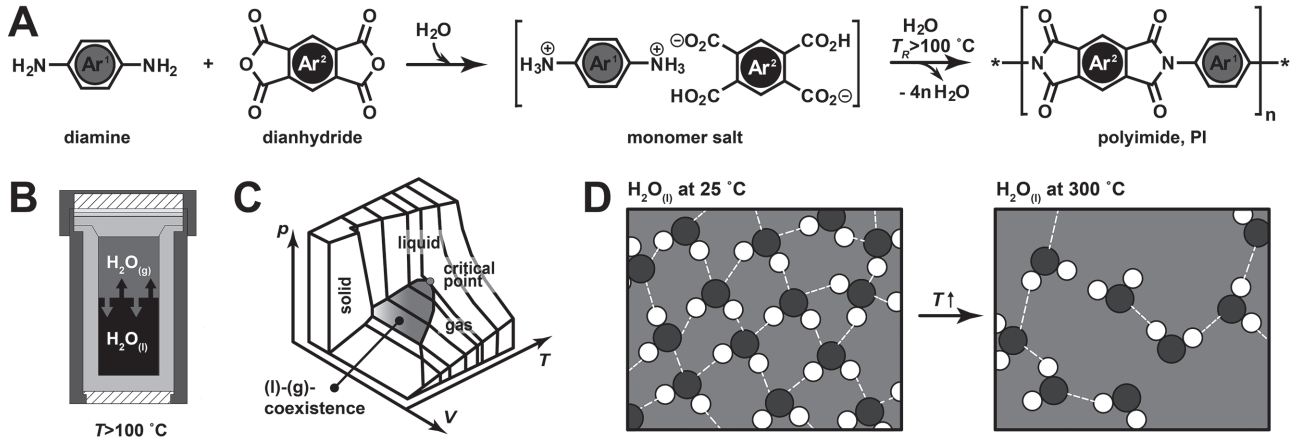

Figure 1. HTP and HTW. A) Reaction equation of HTP of polyimides (right) from the comonomers diamine and dianhydride (left) via monomer salts (middle). B) Schematic of a conventional nonstirred steel autoclave. C) Schematic of the *p*, *T*, *V* phase diagram of pure H_2O. D) Hydrogen-bonding of $H_2O_{(l)}$ at 25 °C (left) vs 300 °C (right).

2.2. Syntheses

2.2.1. Monomer Salt Synthesis

39.26 g of PMDA (180 mmol, 1 eq.) was suspended in 600 mL distilled H_2O and the mixture was degassed by bubbling with Ar for 10 min. The suspension was subsequently heated to 80 °C under Ar atmosphere. After approximately 1 h the hydrolysis of PMDA was complete which gave rise to a clear solution of pyromellitic acid (PMA). The addition of 19.47 g PDA (180 mmol, 1 eq.) immediately leads to precipitation of the monomer salt as an off-white solid. Stirring at 80 °C was continued for 4 h in order to assure full conversion. The obtained $H_2PDA^{2+}PMA^{2-}$ monomer salt was isolated via vacuum filtration and thoroughly washed with distilled H_2O.

^{1}H NMR (250.13 MHz, DMSO-d6): δ [ppm] = 8.42 (2 H, s, Ar_{PMA}-H), 6.79 (4 H, s, Ar_{PDA}-H)

^{13}C NMR (250.13 MHz, DMSO-d6): δ [ppm] = 167.32, 135.29, 133.92, 132.95, 118.89

2.2.2. Hydrothermal Polymerizations

In a typical experiment, 163 mg of the monomer salt $H_2PDA^{2+}PMA^{2-}$ (0.450 mmol, c = 0.03 mol L^{-1}) was placed in a glass liner (V_{liner} = 27 mL) together with 100 mg PEG8000 (c = 6.7 g L^{-1}). 15 mL of distilled H_2O were added and the mixture was thoroughly stirred for 10 min at RT. After removing the stir bar the liner was placed into a PTFE-lined autoclave ($V_{autoclave}$ = 45 mL). The autoclave was put into an oven preheated to 200 °C and kept there for 4 h without stirring. To stop the reaction, the autoclave was quickly cooled back to RT by quenching in cold tap H_2O. The different product phases were separated via pipetting, washed several times with distilled H_2O and subsequently EtOH to finally dry them in vacuo at 80 °C overnight. All other experiments were carried out accordingly and are summarized in the Supporting Information.

2.3. Methods

Attenuated total reflectance Fourier transform infrared (ATR-FT-IR) spectra were recorded on a Bruker Tensor 27 working in ATR MicroFocusing MVP-QL with a diamond crystal, and using OPUS (version 4.0) software for data analysis. The resolution was set to 4 cm^{-1} and spectra were recorded from 4000 to 600 cm^{-1}. ^{1}H and ^{13}C solution NMR spectra were recorded on a Bruker AVANCE 250 (250.13 MHz) equipped with a 5 mm inverse-broad probe head and z-gradient unit. Spectra were analyzed using ACD/NMR processor Academic Edition. PXRD data were collected with a PANalytical X'Pert Pro multi-purpose diffractometer (MPD) in Bragg Brentano geometry operating with a Cu anode at 45 kV, 40 mA, and equipped with a BBHD Mirror and an X-Celerator multichannel detector. Samples were ground and mounted as loose powders on silicon single crystal sample holders. The diffraction patterns were recorded between 5° and 60° (2θ), sample holders were rotated during the measurement with 4 s per turn. Scanning electron microscopy (SEM) was carried out with a Quanta 200F FEI microscope. Typically, the samples were measured at 10 kV with a working distance of 8–10 mm and spot size 2.0. Prior to imaging samples were loaded on carbon-coated stubs and coated by sputtering with a 17 nm thick layer of Au/Pd 60/40 alloy (sputtering current: 30 mA, sputtering time: 60 s) with a Quarum Q105T S sample preparation system.

3. Results and Discussion

For studying the effect of additives during HTP of the polyimide PPPI, we have performed several series of experiments. In the subsequent sections, we first discuss screening experiments employing different additives (Section 3.1), followed by two sets of experiments using PEG8000 as additive (Sections 3.2 and 3.3). Finally, we develop and discuss a hypothesis for the PEG8000-induced morphology alteration of PPPI particles (Section 3.4).

3.1. Screening of Additives during HTP of PPPI

In order to find the additive with the most distinct morphological effect on hydrothermally generated PPPI (**Figure 2**A), we performed a first set of reactions where four different additives (Figure 2B–D) were added to the HTP experiment. Specifically, we tested poly(ethylene glycol) of $\overline{M_n}$ = 400 g mol^{-1} (PEG400) and of $\overline{M_n}$ = 8000 g mol^{-1} (PEG8000), the poly(ethylene glycol)–poly(propylene glycol)–poly(ethylene glycol) triblock copolymer P123 (BASF Pluronic series) and the low-molecular-weight amphiphile CTAB.

Therefore, 0.45 mmol (163.0 mg) of the monomer salt H_2PDA^{2+} PMA^{2-} and 100 mg of the additive were placed in a glass liner and 15 mL of deionized H_2O were added. The mixture was stirred at RT for 10 min, and the glass liner was then transferred to a nonstirred batch autoclave ($V_{autoclave}$ = 45 mL), which was placed in an oven preheated at 200 °C and kept there for 4 h. Then the autoclave was removed from the oven and rapidly quenched in cold tap H_2O to RT. After the HTP reaction, the liner contained three layers (schematically depicted in **Figure 3**A, see Supporting Information for photograph). From bottom to top, a brownish orange *a*-phase, a dark brown *b*-phase, and a translucent supernatant (*c*-phase) of reddish violet color were found. The phases were separated from each other by pipetting and subsequently washed with deionized H_2O and EtOH, and then dried in vacuo at 80 °C. As previously reported, the supernatant *c*-phase is composed of H_2O containing very small amount of strongly colored oligomers formed by the oxidative autopolymerization of PDA.[8] The aspect (color and relative amount) of the reaction mixtures after HTP did not change compared to pristine PPPI (hereafter denoted as "benchmark system") despite the presence of additives: the *a*-phases account for ≈90–95 wt% and the *b*-phases for ≈5–10 wt% of the PPPI product. After drying, all four *a*- and *b*-phases were analyzed by ATR-FT-IR, PXRD, and SEM. ATR-FT-IR confirmed full conversion of the monomer salt to PPPI: the characteristic imide modes were present in all cases and no monomer salt modes (most prominently NH_3^+, CO_2^- and CO_2H modes) could be found (see Figure 3B, representatively shown is the *b*-phase from PEG8000-assisted HTP, for all other additives see Supporting Information). However, in the case of CTAB as additive, we find CH_2 modes in the ATR-FT-IR spectra of PPPI (both *a*- and *b*-phase) that did not vanish even after several thorough washing cycles. Therefrom we conclude that CTAB must be strongly adsorbed or enclosed within the PPPI product. PXRD patterns of the three pure *a*- and *b*- phases are in perfect agreement with the previously reported pattern of PPPI,[8] and no reflections attributed to the monomer salt were found (see Figure 3C).

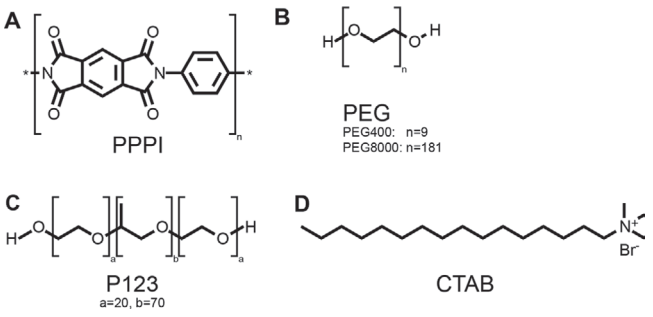

Figure 2. Chemical structures of the synthesized polyimide and employed additives. A) PPPI. B) PEG; with average degrees of polymerization of PEG400 (DP_n = 9) and PEG8000 DP_n = 181). C) Pluronic P123. D) CTAB.

SEM analyses of the four systems reveal morphological differences compared to the additive-free benchmark PPPI (see **Figure 4**). The benchmark system's *a*-phase (Figure 4A) is composed of platelets (≈5–20 µm) that are decorated with smaller platelets to varying extent. The *b*-phase of the benchmark PPPI contains exclusively flower-shaped particles (≈5 µm diameter, Figure 4B). These morphologies are both size- and shape-wise in agreement with previous reports of hydrothermally synthesized PPPI.[8] PPPI synthesized in the presence of PEG400 shows near-spherical microflowers of densely packed roundish petals—sometimes intergrown into bigger agglomerates—and some sparsely decorated platelets in the *a*-phase (Figure 4C). The corresponding *b*-phase contains nondecorated platelets that are either isolated or agglomerated into bigger structures (Figure 4D). In other words: there are no more microflowers present in the *b*-phase when PEG400 is added. When using the higher-molecular weight PEG8000, we again find eventually intergrown near-spherical microflowers of densely packed roundish petals in the *a*-phase (Figure 4E). Moreover, the amount of blank, nondecorated platelets seems to be slightly decreased, which translates into a moderate increase in homogeneity. Interestingly, the corresponding *b*-phase (Figure 4F) is again exclusively containing microflowers of ≈5 µm in diameter that are built up of thin petals with angular edges, as found in the benchmark system (cf. Figure 4A). The low-molecular-weight surfactant CTAB also generates strong morphological changes: Both the *a*- (Figure 4G) and the *b*-phase (Figure 4H) are now composed of randomly oriented small platelets (2–5 µm) and agglomerates thereof. These platelets do not seem to be additionally decorated. Using P123 as additive during HTP, we find microflowers of densely packed roundish petals, which are sometimes agglomerated, and also some sparsely decorated platelets in the *a*-phase (Figure 4I). The *b*-phase is dominated by microflowers (≈5 µm in diameter) with an overall smaller number of petals than in the benchmark *b*-phase (cf. Figure 4B). These microflowers are therefore less dense structures.

In sum, we can conclude that all PPPI products had formed to completion (absence of monomer salt modes as well as no visible end groups in ATR-FT-IR) independent of the type of additive present at the chosen reaction conditions (T_R = 200 °C, t_R = 4 h, $c(H_2PDA^{2+}PMA^{2-})$ = 0.03 mol L^{-1}, c(additive) = 6.7 g L^{-1}). Moreover, the presence of additives during HTP does not influence the crystallinity as judged from PXRD (Figure 3C; Supporting Information). Since PXRD reflects the average crystallinity of randomly oriented crystallites (crystallite grains), the data allow to conclude that the order of PPPI chains within the crystallites is not affected by the presence of additives. However, changes in grain size or shape—which cannot be excluded—cannot be assessed from the obtained PXRD data. In terms of morphology, CTAB generates the strongest morphological difference from the benchmark additive-free PPPI: microflowers are fully absent and we exclusively find small nondecorated

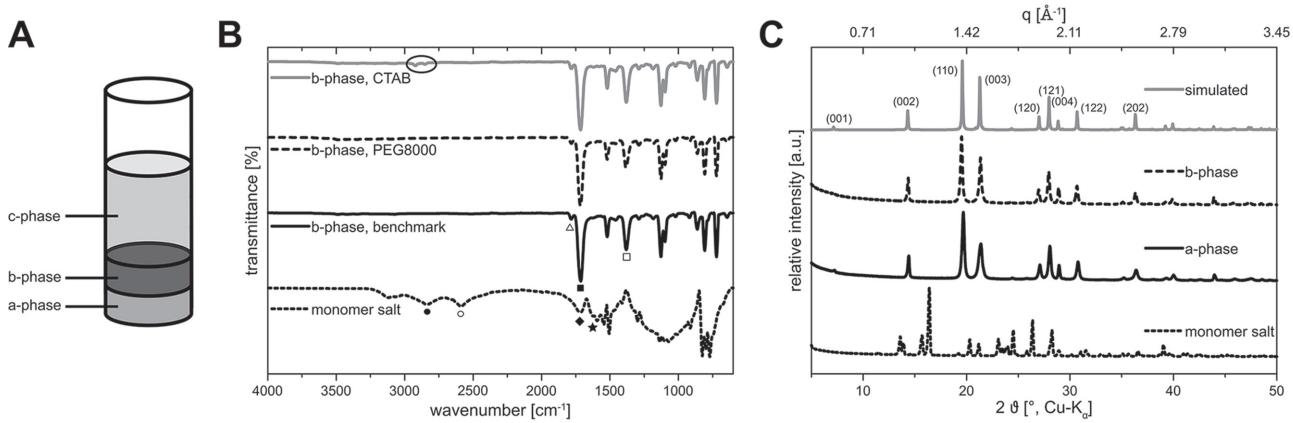

Figure 3. HTP of PPPI–ATR-FT-IR and PXRD of initial additive screening. A) Schematic of a glass liner after HTP. B) ATR-FT-IR spectra of the monomer salt $H_2PDA^{2+}PMA^{2-}$ (bottom) and selected PPPI *b*-phases obtained with *c*(additive) = 6.7 g L^{-1} at T_R = 200 °C and t_R = 4 h using CTAB (top), PEG8000 (second from top) and no additive (third from top). Relevant modes are indicated by symbols. Polyimides: △: C=O,sym imide; ■: C=O,asym imide; □: C—N, imide. Monomer salt: ●: Ar-NH_3^+,sym; ○: Ar-NH_3^+,asym; ◆: C=O, carboxylate; ★: C=O, CO_2H. C) PXRD patterns of the monomer salt (bottom), benchmark PPPI's *a*- and *b*-phase and the pattern simulated using the crystal structure from ref. [8] with all major reflections indicated.

platelets. The obtained platelets correspond to a smaller surface area per particle than in the benchmark's decorated platelets (*a*-phase) and the microflowers (*b*-phase). Moreover, ATR-FT-IR reveals the presence of CH_2 modes from CTAB in both *a*- and *b*-phase that could not be removed even after several thorough washing cycles. This leads to the conclusion that CTAB must be strongly adsorbed by or enclosed in the PPPI particles. The polymeric additives (PEG400, PEG800, and P123) all show similar effects on the morphology of the *a*-phase: In all three cases, we find roundish microflowers of densely packed, lenticular platelets that have curved edges (Figure 4C,E,I). The *b*-phases are composed of microflowers for PEG8000 and P123, and particulate rather inhomogeneous agglomerates for PEG400. For the inhomogeneity and loss of microflower morphologies, we decided to not further pursue the use of PEG400. Due to the (i) positive effects on the morphology of both *a*- and *b*-phase, (ii) the higher solubility in H_2O compared to P123 and (iii) the lower price than P123, we concluded to focus on the use of PEG8000 as additive during HTP for further detailed investigations.

3.2. Effect of PEG8000 Concentration during HTP of PPPI at 200 °C

The selection of PEG8000 as additive-of-choice for morphology modification of PPPI from HTP bears a major preparative advantage: PEG is highly water soluble over a wide range of degrees of polymerization (up to DP_n = 7 million) and over a wide range of concentrations.[15] This allows for preparing

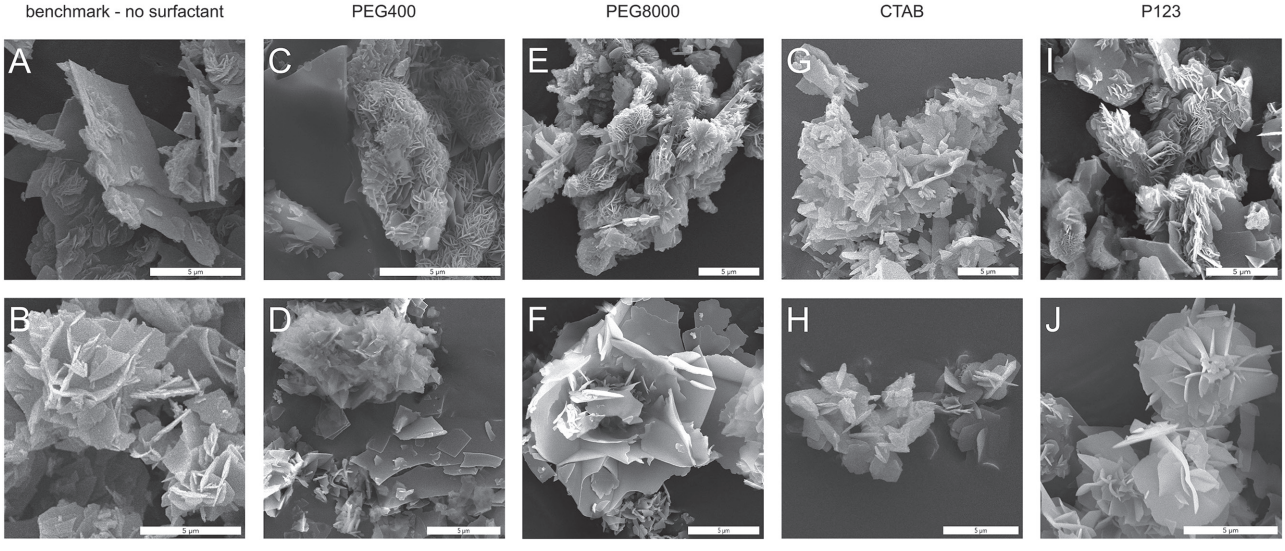

Figure 4. SEM images of PPPI *a*- and *b*-phase of initial additive screening. All samples were polymerized at T_R = 200 °C, t_R = 4 h, *c*($H_2PDA^{2+}PMA^{2-}$) = 0.03 mol L^{-1} and *c*(additive) = 6.7 g L^{-1}. Benchmark PPPI (no additive) A) *a*-phase and B) *b*-phase; C) *a*-phase and D) *b*-phase with PEG400; E) *a*-phase and F) *b*-phase with PEG8000; G) *a*- and H) *b*-phase with CTAB; I) *a*- and J) *b*-phase with P123 as additive.

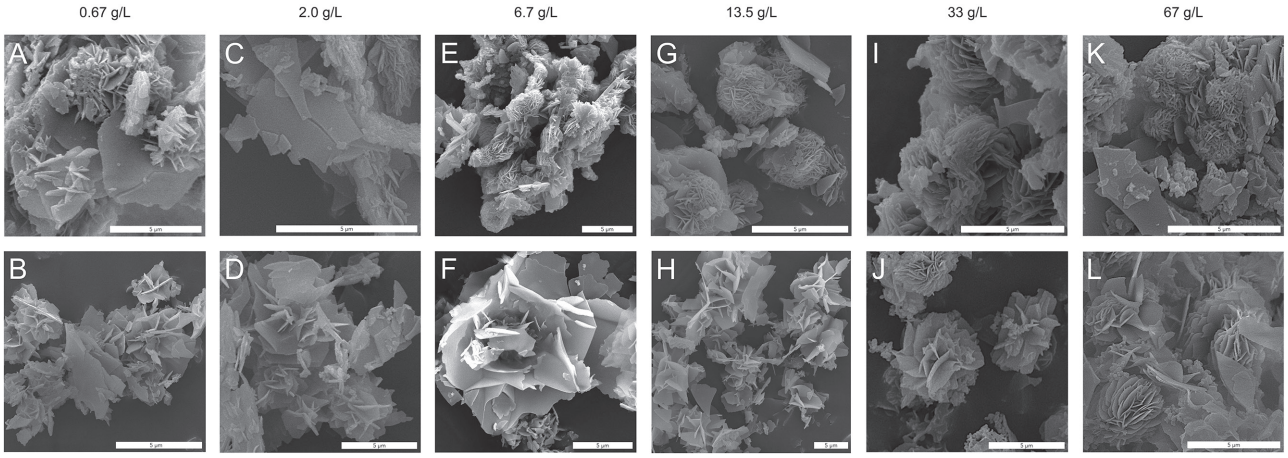

Figure 5. SEM images of PPPI *a*- and *b*-phase using different amounts of PEG8000 during HTP. Polymerization parameters: T_R = 200 °C, t_R = 4 h, $c(H_2PDA^{2+}PMA^{2-})$ = 0.03 mol L^{-1}. *a*- phases: A) [0.67 g L^{-1}], C) [2.0 g L^{-1}], E) [6.7 g L^{-1}], G) [13.5 g L^{-1}], I) [33 g L^{-1}], and K) [67 g L^{-1}]. *b*- phases: B) [0.67 g L^{-1}], D) [2.0 g L^{-1}], F) [6.7 g L^{-1}], H) [13.5 g L^{-1}], J) [33 g L^{-1}] and L) [67 g L^{-1}].

homogeneous aqueous solutions and dispersions of the monomer salt $H_2PDA^{2+}PMA^{2-}$ in these solutions. In order to investigate if and how the PEG8000 content in HTP influences the morphology of PPPI, we performed a concentration study at the same reaction conditions as used for the initial additive screening (T_R = 200 °C, t_R = 4 h, $c(H_2PDA^{2+}PMA^{2-})$ = 0.03 mol L^{-1}. For *c*(PEG8000), we investigated both lower (0.67, 2.0 g L^{-1}) and higher (13.5, 33, 67 g L^{-1}) amounts than initially used in the screening experiments (6.7 g L^{-1}). All PPPI products were fully condensed as judged from ATR-FT-IR (see Supporting Information) and their crystallinity did also not suffer from even the highest PEG8000 concentrations, as can be clearly seen from PXRD (see Supporting Information). At the lowest concentration *c*(PEG8000) = 0.67 g L^{-1}, no significant differences in terms of morphologies of both *a*- and *b*-phase (**Figure 5**A,B)—compared to the benchmark system (see Figure 4A,B)—can be found. At *c*(PEG8000) = 2.0 g L^{-1} the *a*-phase (Figure 5C) is again not influenced as compared to the benchmark system, while the *b*-phase (Figure 5D) shows a slight increase of platelet-shaped particles and a marginal decrease in microflowers. At *c*(PEG8000) = 6.7 g L^{-1}, the morphological impact of the additives starts to become visible. In the *a*-phase roundish microflowers of densely packed lenticular platelets occur—as described earlier (Section 3.2)—while the *b*-phase is comparable to the benchmark system (Figure 4E,F and shown again in Figure 5E,F for clarity). At the next highest concentration, *c*(PEG8000) = 13.5 g L^{-1}, the morphological impact becomes more pronounced. The *a*-phase (Figure 5G) is again composed of microflowers of densely packed roundish, lenticular petals. The petals of these microflowers extend to more or less the same distance from the flower center leading to an increase in perceived sphericity. Moreover, the microflowers are sometimes agglomerated and coexist with a small number of sparsely decorated platelets. Compared to PPPI prepared at 6.7 g L^{-1} PEG8000 (cf. Figure 5E), the amount of blank platelets stays roughly the same. However, more and more isolated (nonagglomerated) dense microflowers start to appear. The *b*-phase (Figure 5H) is now exclusively composed of microflowers. However, one can distinguish between two different types: One resembles the benchmark system's *b*-phase morphologies, while the other type looks similar (but slightly less dense) to the near-spherical microflowers that are found in the *a*-phase of PPPI prepared with *c*(PEG8000) = 13.5 g/L (Figure 5G). At an even higher PEG8000 content of *c*(PEG8000) = 33 g L^{-1} the *a*-phase (Figure 5J) is composed of mostly platelets that are heavily decorated small lenticular platelets. Most interestingly, these small platelets start to show some degree of common directions, i.e., several small platelets are oriented quite parallel to each other.[16] The *b*-phase (Figure 5K) is again (as for 13.5 g L^{-1}) exclusively composed of two types of microflowers: one type similar to the benchmark *b*-phase microflowers, and a second type of near-spherical microflowers featuring lenticular platelets. This second type of microflowers also starts to show common directions in the orientation of the petals, as observed for the *a*-phase. At the highest tested concentration *c*(PEG8000) = 67 g L^{-1}, the amount of undecorated and decorated platelets increases in the *a*-phase (Figure 5K), while the amount of both near-spherical microflowers and common orientation of lenticular platelets decreases. The *b*-phase (Figure 5L) is composed of isolated platelets and near-spherical microflowers showing a high degree of commonly oriented petals.

Indeed, the concentration study shows that the effect of PEG8000 on the morphology of both the *a*- and the *b*-phase of PPPI scales with the amount of PEG. At the highest concentrations of 33 and 67 g L^{-1}, we find an enhanced amount of lenticular platelets that are oriented in a common direction, in both microflowers and decorating platelet-shaped particles. At 33 g L^{-1}, the amount of dense microflowers in the *a*-phase is much increased compared to benchmark PPPI. This is a major improvement, since the *a*-phase is the major product phase. Such a high degree of morphological ordering is to date unprecedented in hydrothermally polymerized aromatic PIs.[8,10,11] At this point—irrespective of the detailed mode-of-action of PEG8000 during HTP—it seemed reasonable to aim for decreasing reaction and crystallization rates of PPPI and thereby check if the impact of PEG8000 could be even stronger. In order to do so, we performed

another set of experiments at a lower reaction temperature, namely at T_R = 180 °C, as the speed of HTP is known to scale with T_R.[8]

3.3. Effect of PEG8000 Concentration during HTP of PPPI at 180 °C

In order to perform PEG8000-assisted HTP of PPPI at 180 °C, we chose to keep the maximum of reaction parameters unchanged by using t_R = 4 h, $c(H_2PDA^{2+}PMA^{2-})$ = 0.03 mol L^{-1} and the same c(PEG8000) that were previously used (2.0, 6.7, 13.5, 33, and 67 g L^{-1}). Moreover, an additive-free PPPI at 180 °C was synthesized for reasons of comparison. Prior to morphological analyses, ATR-FT-IR spectroscopy of all samples was performed and confirmed fully condensed PPPI (see Supporting Information). As for all previous experiments, no changes regarding crystallinity of PPPI were found. All PXRD patterns are in perfect agreement with the literature and show the known reflections of PPPI (see Supporting Information). In the additive-free reference sample the *a*-phase (**Figure 6**A) consists mainly of platelets of ≈5–20 µm, which are in some instances decorated with smaller platelets. The *b*-phase (Figure 6B) is composed of isolated and agglomerated blank platelets (again of 5–20 µm) and some individual, isolated microflowers. Interestingly, the number of microflowers is drastically decreased compared to additive-free PPPI synthesized at T_R = 200 °C. At c(PEG8000) = 2.0 g L^{-1} no significant changes of the *a*-phase (Figure 6C) are observed—compared to the additive-free PPPI (Figure 6A). However, the *b*-phase (Figure 6D) morphology has now changed in favor of an increased number of microflowers. An increase in the amount of PEG to c(PEG8000) = 6.7 g L^{-1} again does not lead to changes in the morphology of the *a*-phase (mainly un- or sparsely decorated platelets of ≈5–20 µm, Figure 6E). In the *b*-phase, we again find microflowers (≈5 µm in diameter) with thin intergrown petals (Figure 6F). Compared to c(PEG8000) = 2.0 g L^{-1} the relative number of microflowers has increased. A further increase of the PEG8000 content to c(PEG8000) = 13.5 g L^{-1} leads to the appearance of small microflowers of densely packed roundish, lenticular petals (≈2–5 µm in diameter) that sometimes agglomerate in the *a*-phase (Figure 6G). In the *b*-phase (Figure 6H), the number of microflowers increases further as compared to all lower PEG concentrations. At the highest PEG8000 concentrations of c(PEG8000) = 33 and 67 g L^{-1}, the *a*-phases (Figure 6I,K) contain denser and bigger near-spherical microflowers (≈5–15 µm in diameter) of densely packed roundish lenticular petals than previously observed. Moreover, the extent to which the flower petals are commonly oriented has further increased compared to PPPI prepared at T_R = 200 °C at those two highest PEG concentrations. In addition, there are almost no more blank platelets observable. In the *b*-phases (Figure 6J,L), we find both isolated near-spherical microflowers with roundish, dense petals and platelets that are decorated with those microflowers. Again, the extent of common orientation of the microflower petals is striking.

Overall, with increasing amount of PEG8000, the effect on the PPPI morphology becomes more pronounced also at T_R = 180 °C. In fact, the extent to which lenticular platelets are oriented in a common direction, both as part of microflowers and decorating bigger platelets, is higher compared to PPPI prepared at 200 °C. Hence, we speculate that the decreased T_R indeed slows down the rates of PPPI formation and crystallization, and therefore allows for a stronger action of PEG. The influence of PEG is exerting morphological control toward denser, near-spherical particles and therefore higher surface areas per particle than in pristine PPPI. In the following and last Section 3.4 of this chapter, we discuss potentially contributing factors and underpinnings of the PEG-induced morphological changes.

3.4. Underpinnings of the Morphology-Altering Effect of PEG during HTP of PPPI

So far this study has shown that the addition of PEG8000 to the HTP of PPPI has an impact on the morphology of the PPPI particles. The morphology alteration is favorable in the sense that the PPPI particles assume higher overall sphericity

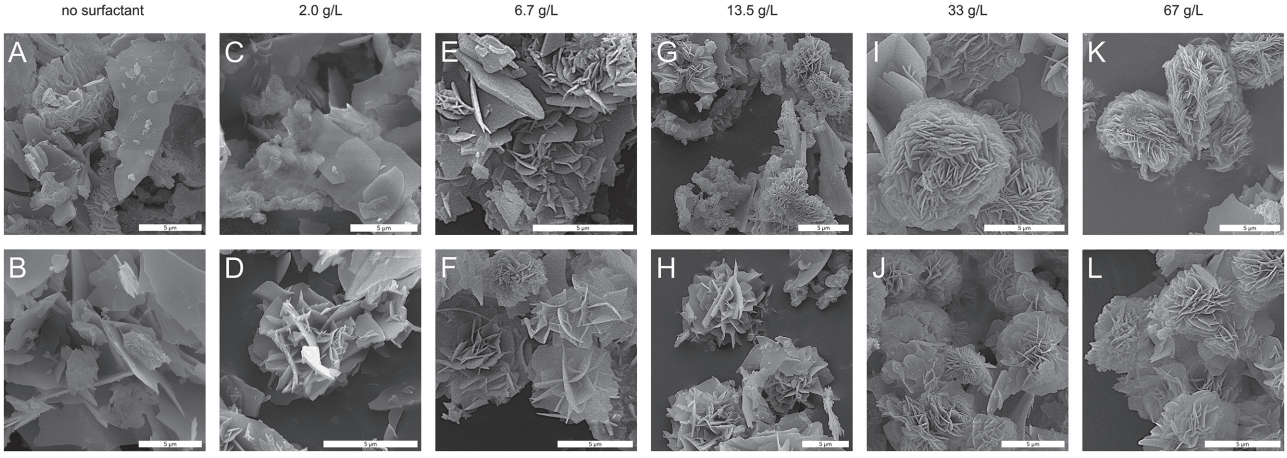

Figure 6. SEM images of PPPI *a*- and *b*-phase using different amounts of PEG8000 during HTP at T_R = 180 °C. Polymerization parameters: t_R = 4 h, $c(H_2PDA^{2+}PMA^{2-})$ = 0.03 mol L^{-1}. *a*- phases: A) (no surfactant), C) [2.0 g L^{-1}], E) [6.7 g L^{-1}], G) [13.5 g L^{-1}], I) [33 g L^{-1}] and K) [67 g L^{-1}]. *b*- phases: B) (no surfactant), D [2.0 g L^{-1}], F) [6.7 g L^{-1}], H) [13.5 g L^{-1}], J) [33 g L^{-1}] and L) [67 g L^{-1}].

by being composed of an increased number of densely packed crystalline platelets. This leads to an enhanced surface area per particle, which is promising for potential applications, e.g., as particle additives in varnishes, where a high contact area with the surrounding medium is desired. In addition, one would expect an increase in mechanical stability in comparison to benchmark PPPI flowers, for the dense packing of the microflower petals. Three major findings become clear from this study: (i) The impact of PEG8000 scales—for both tested T_R of 180 and 200 °C—with its concentration until a certain threshold (i.e., morphologies of samples at c(PEG8000) = 67 g L^{-1} do not vary significantly from those at 33 g L^{-1}). (ii) PEG8000's effect becomes more pronounced at the lower T_R = 180 °C. This suggests that the lower polymerization and crystallization rates give PEG more time to exert morphological alteration. (iii) The PPPI particles retain their global crystallinity. In other words: irrespective of the amount of PEG present during the HTP experiments, PXRD analysis of PPPI particles reflect fully crystalline materials, without any additional reflections or amorphous halos/underground arising and where all reflections perfectly match the experimental and simulated PPPI diffractograms. Especially this last point suggests that in any attempt to rationalize the underpinnings of the observed morphology alterations, one has to treat PPPI as what it is first and foremost: a crystalline material. Therefore, we decided to gather inspiration from scientific fields that deal with the understanding of crystal morphology, i.e., mineralogy and related fields.

Let us first evaluate the morphology of PPPI in additive-free HTP, i.e., the benchmark systems' shapes. PPPI was the first example of a fully crystalline polyimide obtained by HTP.[8] By HTP, but also by other routes,[17–19] PPPI is obtained as highly crystalline powder typically composed of microflower morphologies. In the first publication on PPPI from HTP, we proposed a hypothesis for the arising morphologies, which consists of a monomer salt dissolution–polymerization–crystallization sequence that repeats several times.[8] This means that first, the changed physicochemical properties of $H_2O_{(l)}$ at high-temperatures (namely decreased ε and increased K_W, cf. Section 1) allow for dissolving the at RT water-insoluble monomer salt $H_2PDA^{2+}PMA^{2-}$. Subsequently the comonomers polymerize to PPPI in solution and the PPPI crystallizes on different nucleation sites, including PPPI nuclei, yet nondissolved monomer salt particles, the autoclave wall, or other loci in the reactor. As the monomer salt polymerizes and is hence consumed, further monomer salt can dissolve, polymerize, and crystallize. These cycles repeat until all $H_2PDA^{2+}PMA^{2-}$ is consumed and has formed PPPI. For clarity, this succession is schematically depicted in **Figure 7**A. Moreover, we have suggested, that the final microflower-shape results from a geometrical selection process, i.e., crystalline PPPI sheets act as starting point for the growth of further crystals. New crystallites grow faster if they are initially oriented rather perpendicular to the initial sheet than extend more or less parallel (at a relatively small angle) to the initial sheet. This geometrical selection process is rooted in the fact that the PPPI concentration is higher the further away from the parent sheet, since PPPI that was once close has already been consumed for crystallization (Figure 7B). Indeed, geometrical selection processes are an important cause for the textures of polycrystalline aggregates found in natural minerals.[20] The archetypical mineral exhibiting shapes that resemble the microflowers we observe for benchmark PPPI are so-called desert roses (see Figure 7C), which are evaporites typically composed of barite ($BaSO_4$) and/or gypsum ($CuSO_4.2H_2O$) that incorporate sand grains. As we proposed for PPPI,[8] the morphology of barite roses has been related to "the continuous nucleation and growth of smaller crystals on bigger ones."[21] Recently Schwaiger reported the formation of $Mg(OH)_2$ (brucite) nanoflowers formed by the hydration of MgO cubes.[22] These workers comment that for flower-like morphologies the nucleation is initiated at screw dislocations—independent of the chemical composition. The role of screw dislocations as nucleation sites for new growth layers in crystals is considered the most important case of a growth defect acting as nucleus.[23,24] These reports prompted us to reinvestigate the morphology of benchmark PPPI. When analyzing numerous SEM images of benchmark PPPI, we could identify a reoccurring feature in smaller crystallites growing from bigger platelets: the new crystallites come in pairs of two intergrown platelets that strongly resemble penetration twins (representative SEM with scheme of these structures, see Figure 7D). Since these two platelets that come in an intergrown pair (cf. Figure 7D), we speculate that they are nucleation twins, i.e., simultaneously nucleate and grow. However, the types of twins and their nucleation are various,[25] which clearly make further investigations necessary at this point. Since the secondary petals that we think to be twins are oriented at different angles to the parent sheet (cf. Figure 7D), we believe that their subsequent growth is still subject to a geometrical selection process.

So how can we best understand the role of PEG8000 in the morphological changes? The near-spherical microflowers with densely packed platelets show regions of a high level of alignment between platelets (Figure 6I–L). When drawing a (bent) line in the center of each such commonly oriented region, one again generates an object resembling the benchmark microflowers (Figure 7E). Therefore, we believe that the presence of PEG8000 generates split growth of PPPI platelets, as illustrated in Figure 7F. Such split growth morphologies can be understood as intermediates toward spherulites ("incomplete spherulites"), e.g., bow-tie or sheaf structures.[20] Crystal splitting (or branching) is known for various natural minerals, and synthetic inorganic compounds. In a study on crystal splitting of Bi_2S_3 nanoparticles, Tang and Alivisatos noted that new surface area is generated each time the crystal splits.[26] Moreover, they commented that crystal splitting is found where an organic additive is a very potent surface stabilizer.[26] While, there are alternative possible explanations for crystal splitting in the presence of additives, e.g., noncrystallographic branching,[27] or the formation of mesocrystals,[28] we think that it is indeed the adhesion of PEG8000 molecules to microflower petals, that prohibits the lateral growth of the petals and instead forces them to split for further crystal growth (i.e., adding further PPPI), see Figure 7G. We have currently no proof for this hypothesis. Clearly, further investigations are needed in order to ascertain and deepen this picture of the action of PEG in introducing split growth in PPPI particles.

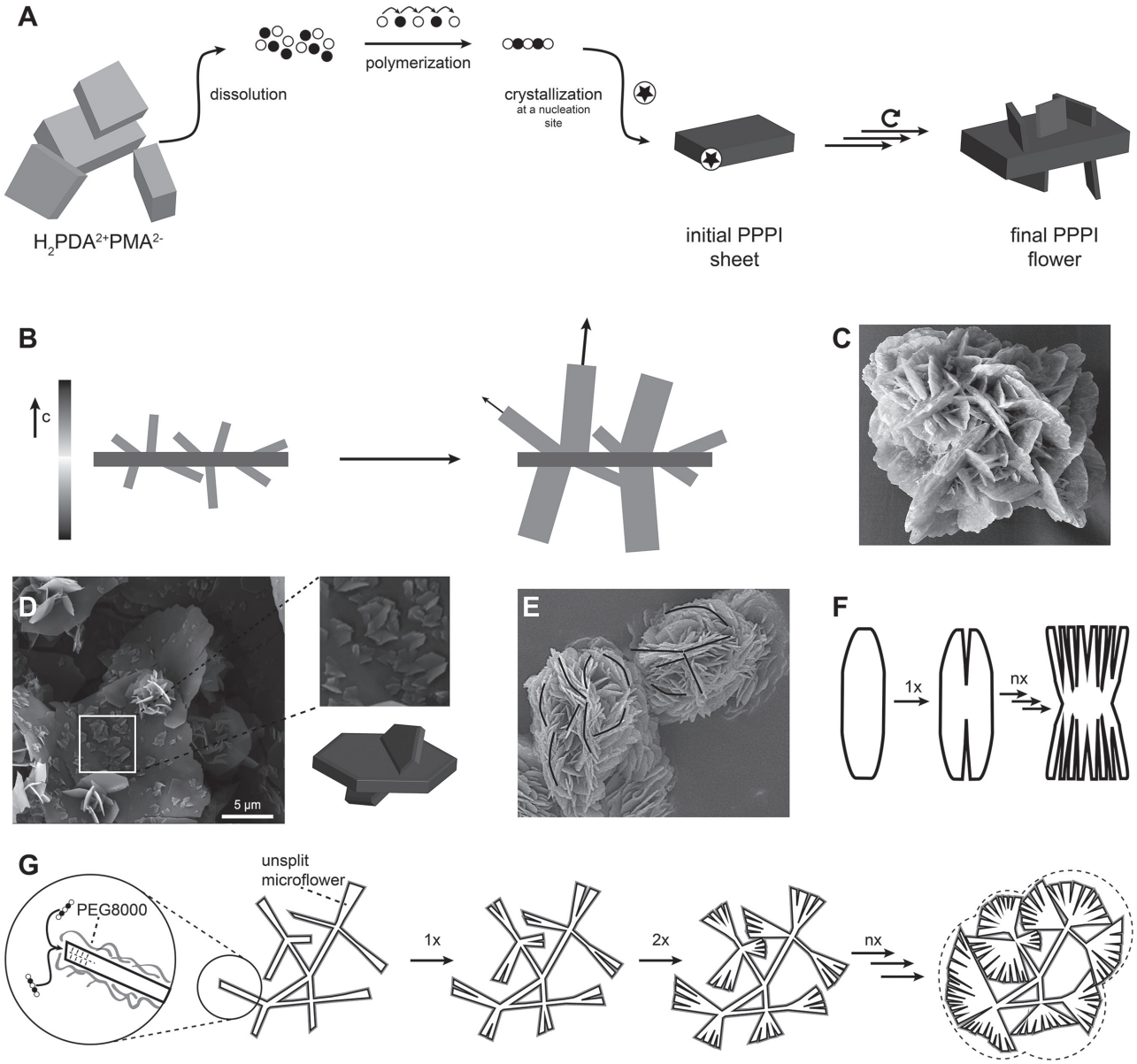

Figure 7. Morphology formation of crystalline PPPI. A) Monomer salt dissolution–polymerization–crystallization sequence; Crystallization nucleus is schematically represented by ✪. Adapted from[8] B) Schematic of microflower formation by geometrical selection: secondary petals perpendicular to parent sheet are closer to regions of higher concentration and hence grow in favor of rather parallel ones. Adapted from[8] C) Photograph of a barite desert rose (by Rama, published under CC license CeCILL). D) SEM image of a PPPI microflower with enlarged view of twin structures and schematic of a penetration twin. E) PPPI microflower obtained in the presence of PEG8000; black lines highlight centers of areas of aligned crystallites. F) Schematic illustration of split growth of a lenticular crystal via a bow-tie shape to a sheaf structure. Adapted from[20] G) Hypothesis on split-growth formation of PPPI microflowers caused by adsorption of PEG to nonsplit microflowers.

4. Conclusions

With this contribution, we have shown that the polyimide PPPI can be obtained hydrothermally in the presence of additives (PEG, Pluronics, and CTAB), without any loss in crystallinity as determined by powder X-ray diffraction. PEG8000 was studied in more detail as additive during HTP. Two concentration studies at two different reaction temperatures (180 °C and 200 °C) show that PPPI crystallinity is retained even at high PEG concentrations. At the same time, the PPPI particle morphologies are affected by the presence of PEG: the initial microflowers transform to more dense microflowers showing areas of oriented sheet-like crystallites. These microflowers are near-spherical and of higher surface area per particle than reference PPPI particles synthesized in the absence of PEG. We attribute these new morphologies to split growth of microflower sheets that is induced by the presence of PEG. In addition, we reevaluated our hypothesis regarding the morphology

formation of pristine PPPI. This leads us to believe that in addition to the previously proposed geometrical selection mechanism twins of PPPI nanocrystallites play a role in the formation of these structures.

Supporting Information

Supporting Information is available from the Wiley Online Library or from the author.

Acknowledgements

The authors are grateful to the Austrian Science Fund (FWF) and the Christian Doppler Research Association (CDG) for funding this project with grant no. PIR 10-N28. Moreover, the authors thank Berthold Stöger for fruitful discussions. X-ray diffraction measurements were carried out at the X-ray Center of TU Vienna, and SEM was performed at the interfaculty electron microscopy facility of TU Vienna (USTEM).

Conflict of Interest

The authors declare no conflict of interest.

Keywords

crystalline polymers, green polymerizations, hydrothermal polymerization, polyimides, polymer morphology

Received: August 2, 2017
Revised: August 21, 2017
Published online: November 9, 2017

[1] S. L. Y. Tang, R. L. Smith, M. Poliakoff, *Green Chem.* **2005**, *7*, 761.
[2] Regulation (EC) No 1907/2006 of the European Parliament and of the Council of 18 December 2006 concerning the Registration, Evaluation, Authorisation and Restriction of Chemicals (REACH) *OJ L* 396, European Commission, **2006**.
[3] CEFIC, EU Chemical Industry Profile 2016, **2016**.
[4] M. M. Unterlass, *Eur. J. Inorg. Chem.* **2016**, *2016*, 1135.
[5] S. Kobayashi, *J. Polym. Sci., Part A: Polym. Chem.* **1999**, *37*, 3041.
[6] M. A. Tehfe, F. Louradour, J. Lalevée, J.-P. Fouassier, *Appl. Sci.* **2013**, *3*, 490.
[7] M. Unterlass, *Biomimetics* **2017**, *2*, 8.
[8] B. Baumgartner, M. J. Bojdys, M. M. Unterlass, *Polym. Chem.* **2014**, *5*, 3771.
[9] M. M. Unterlass, *Mater. Today* **2015**, *18*, 242.
[10] B. Baumgartner, M. Puchberger, M. M. Unterlass, *Polym. Chem.* **2015**, *6*, 5773.
[11] B. Baumgartner, M. J. Bojdys, P. Skrinjar, M. M. Unterlass, *Macromol. Chem. Phys.* **2016**, *217*, 485.
[12] L. Leimhofer, B. Baumgartner, M. Puchberger, T. Prochaska, T. Konegger, M. M. Unterlass, *J. Mater. Chem. A* **2017**, *5*, 16326.
[13] K. Kriechbaum, D. A. Cerrón-Infantes, B. Stöger, M. M. Unterlass, *Macromolecules* **2015**, *48*, 8773.
[14] Note that in a hydrothermal reaction other species are additionally present. Therefore, one actually has to consider a two-phase/multiphase system, which leads to *p*, *T*, *V* characteristics that are different from pure H_2O.
[15] M. Polverari, T. G. M. van de Ven, *J. Phys. Chem.* **1996**, *100*, 13687.
[16] Note that we chose not to use the term "isotropic orientation" for describing the high degree of alignment of the crystallites in order to avaoid confusion with interchain order: In semicrystalline PIs the intermolecular order is often described as isotropic.
[17] K. Wakabayashi, T. Uchida, S. Yamazaki, K. Kimura, *Polymer* **2011**, *52*, 837.
[18] Y. Nagata, Y. Ohnishi, T. Kajiyama, *Polym. J.* **1996**, *28*, 980.
[19] R. Ishige, T. Masuda, Y. Kozaki, E. Fujiwara, T. Okada, S. Ando, *Macromolecules* **2017**, *50*, 2112.
[20] I. Sunagawa, *Crystals: Growth, Morphology and Perfection*, Cambridge University Press, **2005**.
[21] K. Dunn, E. Daniel, P. J. Shuler, H. J. Chen, Y. Tang, T. F. Yen, *J. Colloid Interface Sci.* **1999**, *214*, 427.
[22] R. Schwaiger, J. Schneider, G. R. Bourret, O. Diwald, *Beilstein J. Nanotechnol.* **2016**, *7*, 302.
[23] C. M. Pina, U. Becker, P. Risthaus, D. Bosbach, A. Putnis, *Nature* **1998**, *395*, 483.
[24] L. G. Benning, G. A. Waychunas, in *Kinetics of Water-Rock Interaction*, Springer, New York **2008**, p. 259.
[25] T. Hahn, H. Klapper, *International Tables for Crystallography*, Vol. D, Kluwer Academic Publishers, Dordrecht, Netherlands **2006**, p. 393.
[26] J. Tang, A. P. Alivisatos, *Nano Lett.* **2006**, *6*, 2701.
[27] A. G. Shtukenberg, Y. O. Punin, E. Gunn, B. Kahr, *Chem. Rev.* **2011**, *112*, 1805.
[28] H. Cölfen, M. Antonietti, *Mesocrystals and Nonclassical Crystallization*, John Wiley & Sons, Chichester, England **2008**.